RSC Advances

PAPER

View Article Online
View Journal | View Issue

Cite this: *RSC Adv.*, 2019, **9**, 27147

Decorated single-enantiomer phosphoramide-based silica/magnetic nanocomposites for direct enantioseparation†

Fatemeh Karimi Ahmadabad, [a] Mehrdad Pourayoubi *[a] and Hadi Bakhshi [b]

Received 1st May 2019
Accepted 16th August 2019

DOI: 10.1039/c9ra03260f

rsc.li/rsc-advances

The nano-composites Fe_3O_4@SiO_2@(−$O_3Si[(CH_2)_3NH]$)P(=O)(NH-*R*(+)$CH(CH_3)(C_6H_5)$)$_2$ (Fe_3O_4@SiO_2@PTA(+)) and Fe_3O_4@SiO_2@(−$O_3Si[(CH_2)_3NH]$)P(=O)(NH-*S*(−)$CH(CH_3)(C_6H_5)$)$_2$ (Fe_3O_4@SiO_2@PTA(−)) were prepared and used for the chiral separation of five racemic mixtures (PTA = phosphoric triamide). The separation results show chiral recognition ability of these materials with respect to racemates belonging to different families of compounds (amine, acid, and amino-acid), which show their feasibility to be potential adsorbents in chiral separation. The nano-composites were characterized by FTIR, TEM, SEM, EDX, XRD, and VSM. The VSM curves of nano-composites indicate their superparamagnetic property, which is stable after their use in the separation process. Fe_3O_4, Fe_3O_4@SiO_2, Fe_3O_4@SiO_2@PTA(+) and Fe_3O_4@SiO_2@PTA(−) are regularly spherical with uniform shape and the average sizes of 17–20, 18–23, 36–47 and 43–52 nm, respectively.

Introduction

Chirality is a major concern in modern pharmaceuticals,[1,2] pesticides,[3] flavorings,[4] food additives,[5] non-linear optical materials[5,6] and asymmetric catalysis.[7–10] Chiral recognition/resolution is of great interest and ever-increasing importance, thus large efforts have been made towards techniques suitable for this aim such as chromatography,[11–14] enzyme resolution,[15] membrane separation,[16–18] and chemical recognition.[19] In this regard, the applications of chiral materials/chiral selectors in the enantioseparations based on the formation of different diastereomeric adducts, were studied,[20–24] and the interactions such as hydrogen bonding, hydrophobic/hydrophilic, π–π, dipole–dipole, and ionic were reported in the adduct formation.[25–28]

Since their discovery, silica-based materials have emerged as a source of immense potential for applications like for example in selective adsorption, separation, catalysis, and preparation of novel functional materials.[29–36] Chemically modifiable surfaces and superparamagnetic property of magnetic modified silica nanoparticles have attracted much attention.[31,37–41] The usefulness of magnetic adsorbents is due to their easily and rapidly separation under an external magnetic field, and in such purposes Fe_2O_3 nanorods, Fe_3O_4 and Fe–Pt alloy nanoparticles, and Fe_3O_4–polymer composites were studied.[41–49] Recently, with regard to chiral discrimination, some magnetic nano-structured materials decorated with appropriate chiral molecules have been inspected.[50–56] Typical examples are Fe_3O_4@SiO_2@PNCD and Fe_3O_4@SiO_2@CBDMPC, where the chiral selectors PNCD and CBDMPC are substituted β-cyclodextrin and cellulose, respectively, and their most important functional groups are OH and ether oxygen. Direct separation of enantiomers *via* such decorated magnetic nanomaterials would show great advantages compared with traditional methods of chiral separation.[29,57] One example is the application of *R*(+)-α-methylbenzylamine-modified magnetic chiral sorbent in enantioseparation of mandelic acid.[58]

From our previous studies on phosphorus–oxygen, phosphorus–nitrogen and phosphorus–sulfur compounds,[59–64] the P=O group was found as the best hydrogen-bond acceptor with respect to the other possible acceptor groups which usually exist in the molecules, typically C=O, S=O, N–O, P=S, ester and ether oxygen atoms, nitrogen, and π-system, examined with X-ray diffraction study, statistical analysis based on the data deposited in the Cambridge Structural Database (CSD)[65,66] and quantum chemical calculations in some cases. The structures investigated include both achiral and chiral phosphorus compounds.[63,67–70]

With this background in mind, in the current article, we synthesized chiral phosphoramide enantiomers including Si–OCH_3 segment in the achiral moiety, which is sensitive to hydrolysis condensation. This characteristic helps to immobilize silicon-based chiral phosphoric triamide (PTA) on Fe_3O_4@SiO_2, to produce composite materials which dually possess the chiral and superparamagnetic properties. The target materials include the P=O functional group which allows acting as a good selector, due to relatively strong interactions with OH

[a]*Department of Chemistry, Faculty of Science, Ferdowsi University of Mashhad, Mashhad, Iran. E-mail: pourayoubi@um.ac.ir*

[b]*Macromolecular Chemistry II, University of Bayreuth, Universitätsstraße 30, 95440 Bayreuth, Germany*

† Electronic supplementary information (ESI) available. See DOI: 10.1039/c9ra03260f

and NH units. The full characterizations of prepared composites and their behavior as adsorbents in direct enantioseparation have been investigated.

Experimental

Materials

Phosphoryl chloride ($POCl_3$, 99%), (*R*)-(+)-α-methylbenzylamine (*R*MBA, 98%), (*S*)-(−)-α-methylbenzylamine (*S*MBA, 98%) and (±)-α-methylbenzylamine (MBA, 98%) were bought from Sigma-Aldrich. Methanol, ethanol, tetrahydrofuran (THF), sodium chloride (NaCl), ferric chloride hexahydrate ($FeCl_3 \cdot 6H_2O$), ferrous chloride tetrahydrate ($FeCl_2 \cdot 4H_2O$), ammonium hydroxide (25% (w/w)), glycerol, tetraethyl orthosilicate (TEOS), 3-aminopropyltrimethoxysilane (APTMS), DL-tartaric acid (99%), DL-phenylalanine (99%), DL-valine (99%) and triethylamine (TEA, 99%) were purchased from Merck.

Instruments

Fourier transformed infrared (FTIR) spectra were obtained by a Buck scientific spectrometer (model EQUINOX 55) using KBr disks. The size and morphology of nanoparticles were monitored using a transmission electron microscope (TEM) from Leo (model 920 AB) with accelerating voltage of 35 kV and resolution of 1 nm. A Tescan instrument (model Mira) was also used for scanning electron microscopy (SEM) with an accelerating voltage of 35 kV and a resolution of 4 nm. Energy-dispersive X-ray spectroscopy (EDX) was performed by an Oxford Instrument (model INCA). XRD patterns were recorded by a Bruker instrument (model D8 Advance) using Ni-filtered Cu Kα radiation. ^{31}P, ^{1}H- and ^{13}C-nuclear magnetic resonance (NMR) spectra were recorded on a Bruker instrument (model Avance 300) using DMSO-d_6/THF and $CDCl_3$/CH_3OH/H_2O as solvents. Circular dichroism (CD) measurements were carried out on an Aviv circular dichroism spectrometer (model 215) using solutions in THF (5 g L^{-1}). Magnetic susceptibility measurements were carried out using a vibrating sample magnetometer (VSM) (BHV-55, Riken, Japan) in the magnetic field range from −8000 to 8000 Oe at room temperature.

Synthesis of single-enantiomer phosphoric triamides

The procedures for the synthesis of P(=O)(NH-*R*-(+)CH(CH_3)C_6H_5)$_2$(NH$(CH_2)_3$Si$(OCH_3)_3$), PTA(+), and P(=O)(NH-*S*-(−)CH(CH_3)C_6H_5)$_2$(NH$(CH_2)_3$Si$(OCH_3)_3$), PTA(−), are similar and the only difference is related to the enantiomeric form of amine used. Therefore, the procedure is typically described for PTA(+) as follows: a solution of *R*MBA (4.6 mmol) and TEA (4.6 mmol) in dry THF (15 mL) was added dropwise to a stirring solution of $POCl_3$ (2.3 mmol) in dry THF (10 mL) at 0 °C. After stirring for 5 h, the obtained white solid (triethylammonium chloride salt) was filtered off and a solution of APTMS (2.3 mmol) and TEA (2.3 mmol) in dry THF (10 mL) was added dropwise to the filtrate at 0 °C. After stirring for 4 h, the generated triethylammonium chloride salt was filtered off. Since the Si$(OCH_3)_3$ moiety of PTA was moisture sensitive, a few amounts of THF solution were directly used for the NMR measurements, after adding two droplets of DMSO-d_6 to the NMR tube for adjustment requirement. Finally, the THF solvent was removed under vacuum and the prepared phosphoric triamide was used for the synthesis of Fe_3O_4@SiO_2@PTA. $[\alpha]_D^{RT}$ (in dry THF, 5 g L^{-1}) = +34.1°. Selected peaks in FTIR (cm^{-1}): 3396, 3248 (N–H), 3028 (C–$H_{aromatic}$), 2949 (C–H), 2844, 1190 (P=O), 1082 (Si–O). $^{31}P\{^1H\}$-NMR (THF/DMSO-d_6, ppm): 13.35. $^{13}C\{^1H\}$-NMR (THF/DMSO-d_6, ppm): 6.42 (s, C_2), 21.63 (s, C_{6+11}), 23.76 (s, C_{6+11}), 25.09 (d, C_3, $^3J_{P-C}$ = 6.5 Hz), 46.22 (s, C_4), 50.10–50.90 (C_1, C_{5+12}), (126.26, 126.35, 126.62, 128.10, 128.53) ($C_{8-10,14-16}$), 146.44 (d, C_{7+13}), 147.70 (d, C_{7+13}, $^3J_{P-C}$ = 7.2 Hz). ^1H-NMR (THF/DMSO-d_6, ppm): 0.56 (m, 2H, CH_2), 1.38 (m, 6H, CH_3), 1.57 (m, 2H, CH_2), 2.02 (m, 2H, CH_2), 3.40 (t, 1H, NH), 3.48 (m, 9H, CH_3), 3.88 (t, 1H, NH), 3.98–4.22 (m, 2H, CH), 4.28 (b, 1H, NH), 7.15–7.50 (10H, C–$H_{aromatic}$).

Preparation of chiral phosphoramide-modified hybrid magnetic/silica nanoparticles, Fe_3O_4@SiO_2@PTA(+) and Fe_3O_4@SiO_2@PTA(−)

Fe_3O_4, as nanoparticles, was prepared according to a previously reported method[72] as follows: to a solution of $FeCl_3 \cdot 6H_2O$ (8.6 mmol) and $FeCl_2 \cdot 4H_2O$ (4.3 mmol) in H_2O (40 mL) at 85 °C, NH_3 (3 mL, 25%) was added (under bubbling of N_2 gas). After 20 min, the magnetic nanoparticles were separated and washed with an aqueous solution of NaCl (0.02 M, 50 mL) and then twice with deionized water (2 × 50 mL), followed by drying under vacuum at 60 °C for 5 h.

Fe_3O_4@SiO_2 was prepared according to a published sol–gel method.[72] The synthesis procedure is as follows: Fe_3O_4 (1 g) was dispersed in deionized water (100 mL) under ultrasonication for 10 min. After that, an aqueous solution of TEOS (10% v/v, 100 mL) and then glycerol (50 mL) were added to this mixture. The pH was adjusted to 4.5 by using glacial acetic acid and the reaction mixture was stirred continuously for 2 h at 90 °C. The product was separated with a magnet and then washed four times with ethanol. Finally, the obtained Fe_3O_4@SiO_2 was dried under vacuum at 60 °C for 6 h.

At the end step, chiral phosphoric triamide was deposited on the Fe_3O_4@SiO_2 nano-composite. The procedures are similar for deposition of PTA(+) or PTA(−) and typically is given for PTA(+). For this aim, Fe_3O_4@SiO_2 (2 g) was ultrasonicated in ethanol (50 mL) for 10 min, then PTA(+) (0.5 g) in 2 mL ethanol was added under nitrogen atmosphere and the mixture refluxed for 12 h. After, the residue (Fe_3O_4@SiO_2@PTA(+)) was magnetically separated and washed with methanol/H_2O. The condensation of Si–OCH_3 in phosphoric triamide and Si–OH in Fe_3O_4@SiO_2 leads to deposition through the formation of Si–O–Si linkage.

Methods

Specific rotations of PTA(+) and PTA(−), [α], were measured with an automatic digital polarimeter (WZZ-2B, sodium lamp), using solutions in THF (5 g L^{-1}), according to the following equation:

$$[\alpha] = \alpha/(L \times c) \quad (1)$$

where α is the measured optical rotation in degree, L is the path length in decimetre, and c is the concentration in g/100 mL.

Dextrorotation and levorotation are identifying by (+) and (−), respectively.

The averages of particle sizes for nano-adsorbents were calculated by using the Scherrer equation, as follows:[71]

$$D = K\lambda/\beta \cos\theta \quad (2)$$

where K is a constant in the range of 0.89–1.39 depending on the particle morphology and set as 0.90, λ is the wavelength of the radiation, β is the full-width at half-maximum (FWHM) and θ is the diffraction angle.

Fe_3O_4@SiO_2@PTA(+) and Fe_3O_4@SiO_2@PTA(−) were examined for chiral separation of five racemic mixtures, *i.e.*, (±)-α-methylbenzylamine, DL-tartaric acid, DL-alanine, DL-phenylalanine, and DL-valine. For this aim, 1 g adsorbent was mixed with 25 mL solution of each racemic mixture (5 g L^{-1}) in H_2O/CH_3OH (80/20, v/v). The mixture was continuously stirred for 1 h. After that, the adsorbent was collected with a magnet and the optical purity of supernatant was determined through measuring its optical rotatory according to the following equation:[52,53]

$$\text{Optical purity} = [\alpha]_{\text{supernatant}}/[\alpha]_{\text{pure enantiomer}} \quad (3)$$

Results and discussion

Syntheses, spectroscopic features and optical properties of PTA(+) and PTA(−)

The route of synthesis and chemical structure of P(=O)(NH-*R*-(+)$CH(CH_3)C_6H_5)_2(NH(CH_2)_3Si(OCH_3)_3)$, PTA(+), and P(=O)(NH-*S*-(−)$CH(CH_3)C_6H_5)_2(NH(CH_2)_3Si(OCH_3)_3)$, PTA(−), are shown in Fig. 1a and b. For the synthesis of these chiral compounds, the prepared reagents P(=O)(NH-*R*-(+)$CH(CH_3)C_6H_5)_2$Cl and P(=O)(NH-*S*-(−)$CH(CH_3)C_6H_5)_2$Cl were treated with APTMS in order to the replacement of Cl atom by $(CH_3O)_3Si(CH_2)_3NH$ moiety in the presence of triethylamine as an HCl scavenger. The P–Cl bond in the reagent and Si–OCH_3 bond in PTA are moisture sensitive; hence, dry THF was used as the reaction medium. The usefulness of this solvent is also related to the high solubility of chiral reagent and chiral product and the low solubility of the triethylammonium chloride salt, which allows to a nearly clean reaction and easy purification.

It should be noted that the removing of triethylammonium chloride salt (or other organic salt depending on HCl scavenger used) can be done by H_2O for the phosphoramides non-sensitive to moisture.[68,73] For the water-sensitive compounds, a solvent with different solubilities of phosphoramide and organic salt is used. For examples, the syntheses of moisture-sensitive phosphoramides rac-XP(=O)(OC_6H_5)(Cl) [X = $(NHC_6H_4$-*p*-$CH_3)$ and (NH-cyclo-C_6H_{11})] were reported[68] in dry chloroform, with low solubilities of *p*-toluidine hydrochloride and cyclohexylamine hydrochloride salts and high solubilities of phosphoramides. Moreover, the synthesis of P(=O)(NH-*R*-(+)$CH(CH_3)C_6H_5)_2$Cl and P(=O)(NH-*S*-(−)$CH(CH_3)C_6H_5)_2$Cl have been reported.[63]

The FTIR spectrum of PTA is shown in Fig. 1c, the characteristic peaks of N–H, C–H, P=O and Si–O bonds confirm the correctness of the structure. In the $^{31}P\{^1H\}$ NMR spectrum (Fig. S1†) a singlet is observed at 13.35 ppm in comparison with the value of 3.75 ppm (in DMSO-d_6) for [2,6-F_2-$C_6H_3C(O)NH$][*R*-(+)$(C_6H_5)CH(CH_3)NH]_2P(=O)$, which is a closely related phosphoric triamide published in point of view of the chiral amine used.[74]

The specific rotations of P(=O)(NH-*R*-(+)$CH(CH_3)C_6H_5)_2$-$(NH(CH_2)_3Si(OCH_3)_3)$ and P(=O)(NH-*S*-(−)$CH(CH_3)C_6H_5)_2$-$(NH(CH_2)_3Si(OCH_3)_3)$ were obtained as +34.1° and −33.5°, respectively. The circular dichroism (CD) spectra of these two enantiomers are shown in Fig. 1d. The CD spectra exhibit opposing signals, a negative peak with a minimum at 260 nm belonged to PTA(+) and a positive peak with a maximum at 252 nm for PTA(−). On the other hand, the CD patterns are almost mirrored images with respect to one another in the range of 200–400 nm.

In the $^{13}C\{^1H\}$-NMR spectrum (Fig. 2a), two sets of signals are observed for the carbon atoms of two $NHCH(CH_3)C_6H_5$ groups. Typically, two singlets at 21.63 and 23.76 ppm are related to methyl carbon atoms and two doublets at 146.44 and 147.70 ppm correspond to the *ipso*-carbon atoms. The corresponding peaks for the $(CH_3O)_3SiCH_2CH_2CH_2$ moiety are the singlets at 6.42, 46.22 and 50.10 ppm and a doublet at 25.09 ppm. The *ortho*, *meta* and *para* carbon atoms of two phenyl rings appear in the range of 126.26–128.53 ppm. For the assignment of the signals of chiral amine, the NMR spectra of [2,6-F_2-$C_6H_3C(O)NH$][*R*-(+)$(C_6H_5)CH(CH_3)NH]_2P(=O)$[74] were inspected and for the assignment of the signals of silicon-based amine, the NMR spectra of Fe_3O_4@SiO_2@–$O_2(OCH_3)Si[(CH_2)_3NH_2]$[75] and the newly synthesized $((CH_3O)_3SiCH_2CH_2$-$CH_2NH)P(=O)(OC_6H_5)_2$ compound were investigated. The structure, details of the synthesis procedure of $((CH_3O)_3SiCH_2$-$CH_2CH_2NH)P(=O)(OC_6H_5)_2$ and NMR data are given in the ESI (Fig. S2–S5†). The ^{1}H-NMR spectrum shows the characteristic peaks for chiral and silicon-based amine fragments, which includes the signals at 0.56, 1.57, 2.02 and 3.48 ppm (multiplets) and at 4.28 ppm (broad) related to three CH_2, CH_3 groups and one NH for silicon-based amine, and the signals at 1.38, 3.40, 3.88 and 3.98–4.22 ppm, respectively for CH_3, two NH units and CH groups of the chiral amine segments. The aromatic protons appeared at 7.15–7.50 ppm (Fig. 2b).

Syntheses and characterization of Fe_3O_4@SiO_2@PTA(+) and Fe_3O_4@SiO_2@PTA(−)

The Fe_3O_4 nanoparticles were prepared by precipitation from iron(II) and (III) ions in a basic solution under nitrogen atmosphere and then coated with a thin silica layer, formed by hydrolysis and condensation of TEOS in an acidic alcohol/water solution *via* a sol–gel process. Then, the immobilization of the chiral selector was carried out through the formation of Si–O–Si linkage,[76] between the silica layer and silicon-based chiral selector. The procedure for the preparation of Fe_3O_4@SiO_2@PTA(+) and Fe_3O_4@SiO_2@PTA(−) is illustrated in Scheme 1.

FTIR

Grafting of chiral phosphoric triamide on Fe_3O_4@SiO_2 was verified by FTIR. The FTIR spectra of Fe_3O_4, Fe_3O_4@SiO_2, and

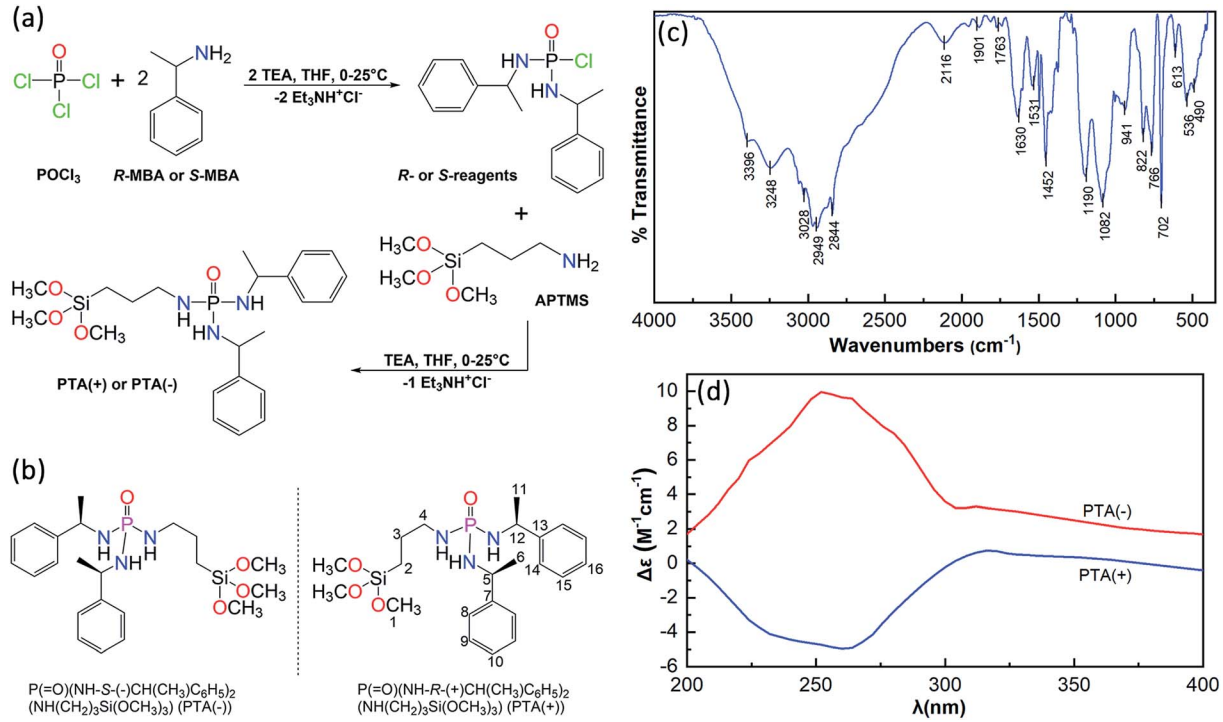

Fig. 1 Synthesis route (a), chemical structure (b), FTIR spectrum (c) and CD spectra (d).

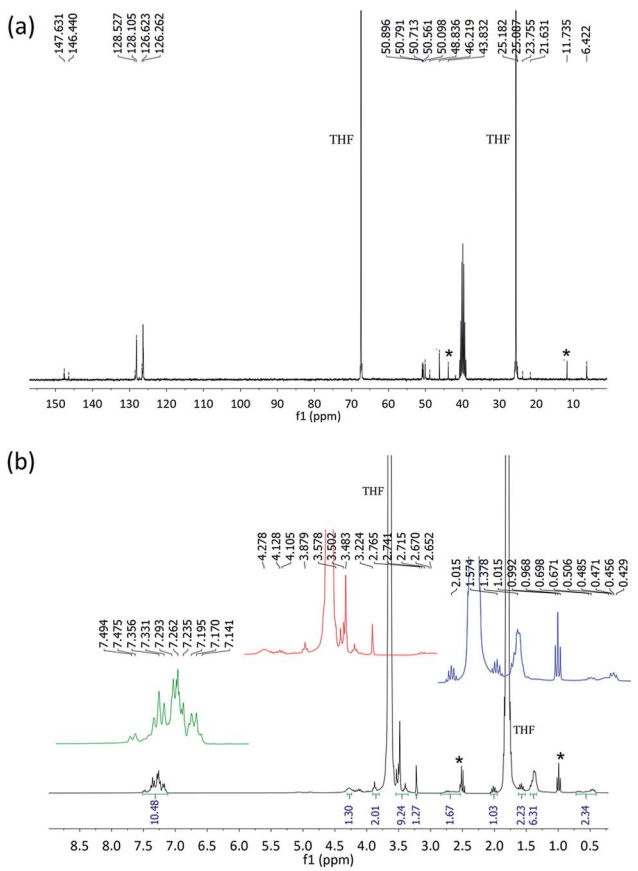

Fig. 2 The ^{13}C-NMR (a) and ^{1}H-NMR (b) spectra of PTA. The peaks marked with * are related to triethylammonium chloride.

Fe_3O_4@SiO_2@PTA(+) are shown in Fig. 3, respectively. In all spectra, the broad peak in the range of 540–578 cm^{-1} is attributed to the Fe–O vibration. For silicon-containing nanoparticles, the strong and broad bands at about 1000–1100 cm^{-1} demonstrate the presence of Si–O–Si and Si–OH stretching vibrations.[77,78] In the IR spectrum of Fe_3O_4@SiO_2@PTA(+), the band at 1214 cm^{-1} is related to the P=O stretching vibration of PTA(+) and the peaks in the range 2840–3248 cm^{-1} are related to C–H and N–H stretches. These peaks confirmed the occurrence of immobilization.

VSM

The magnetic properties of Fe_3O_4, Fe_3O_4@SiO_2, and Fe_3O_4@SiO_2@PTA were studied by the hysteresis loops at room temperature by using vibrating sample magnetometry (VSM), with the magnetization curves as shown in Fig. 4. The

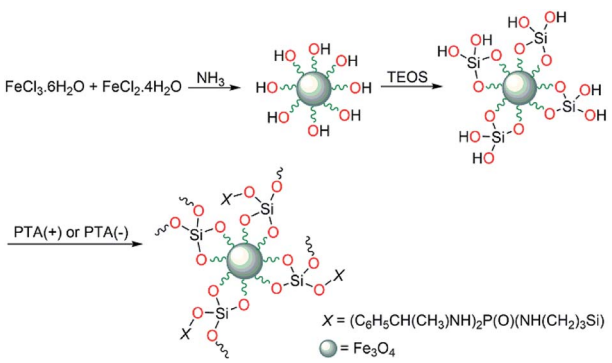

Scheme 1 Preparation steps for the fabrication of Fe_3O_4@SiO_2@PTA.

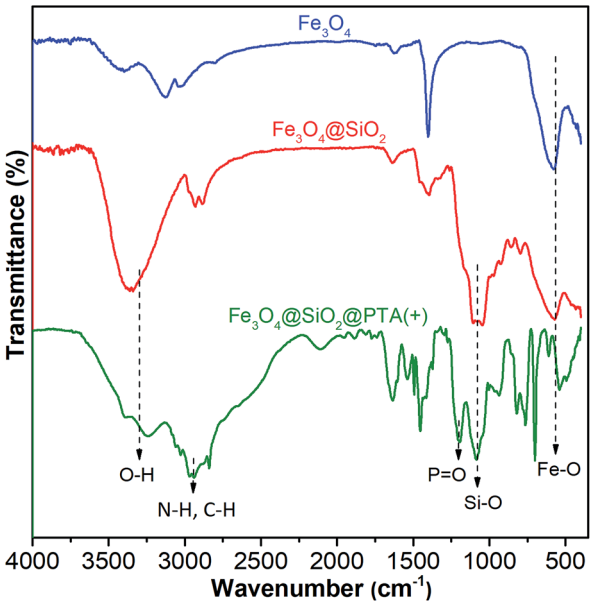

Fig. 3 The FTIR spectra of Fe_3O_4, Fe_3O_4@SiO_2, and Fe_3O_4@SiO_2@PTA(+).

magnetization curves exhibited superparamagnetic properties of Fe_3O_4 and Fe_3O_4@SiO_2 with the saturation magnetizations of about 80 emu g^{-1} and 76 emu g^{-1}, respectively. For Fe_3O_4@SiO_2@PTA(+), the saturation magnetizations were measured before and after using in the chiral separation process, giving to be about 47 emu g^{-1} and 45 emu g^{-1}, respectively, showing the stability of superparamagnetic property during the separation process.

XRD

The crystalline structures of Fe_3O_4, Fe_3O_4@SiO_2, Fe_3O_4@SiO_2@PTA(+) and Fe_3O_4@SiO_2@PTA(−) were analyzed *via* XRD (Fig. 5). Characteristic diffraction peaks for Fe_3O_4 were observed at 30.1° (202), 35.5° (311), 43.1° (400), 53.6° (422), 57° (511), 62.6° (440), 71° (602) and 74° (533), in agreement with the crystalline cubic spinel Fe_3O_4 structure (JCPDS no. 19-0629).[79] The similar characteristic peaks observed for Fe_3O_4@SiO_2, Fe_3O_4@SiO_2@PTA(+) and Fe_3O_4@SiO_2@PTA(−) indicated the stability of the crystalline phase of Fe_3O_4 in the composite materials. The averages of particle sizes for nano-composites were calculated by using the Scherrer equation, which yielded the values of 17, 18, 36 and 43 nm for Fe_3O_4, Fe_3O_4@SiO_2, Fe_3O_4@SiO_2@PTA(+) and Fe_3O_4@SiO_2@PTA(−), respectively, in good agreement with microscopy results. The expanded XRD spectra and related details have been shown in Fig. S6–S9.†

TEM, SEM, and EDX

The morphologies of Fe_3O_4, Fe_3O_4@SiO_2, Fe_3O_4@SiO_2@PTA(+) and Fe_3O_4@SiO_2@PTA(−) were identified with SEM and TEM, as shown in Fig. 6. The images exhibit a nearly mono-dispersed structure for Fe_3O_4, with a rough surface because of the numerous reunited nanoparticles. After coating with SiO_2, the surface of nanoparticles became smooth, and a SiO_2 layer was observed around the Fe_3O_4 core. Deposition of chiral phosphoric triamide causes an increase in the particles' diameters. The averages of particle sizes are about 20, 23, 47 and 52 nm for Fe_3O_4, Fe_3O_4@SiO_2, Fe_3O_4@SiO_2@PTA(+) and Fe_3O_4@SiO_2@PTA(−), respectively.

EDX spectra of Fe_3O_4, Fe_3O_4@SiO_2, Fe_3O_4@SiO_2@PTA(+) and Fe_3O_4@SiO_2@PTA(−) were recorded. In Fe_3O_4@SiO_2@PTA(+) and Fe_3O_4@SiO_2@PTA(−) nanocomposites energetic lines for silicon, iron, carbon, oxygen, and phosphorus have been observed that confirm the immobilization of chiral selectors on the surface of Fe_3O_4@SiO_2 (Fig. 7).

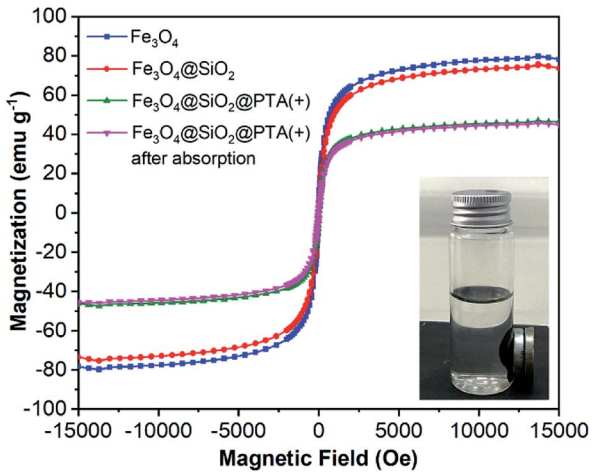

Fig. 4 Magnetization curves for Fe_3O_4, Fe_3O_4@SiO_2, and Fe_3O_4@SiO_2@PTA(+) nanoparticles before and after using as an adsorbent.

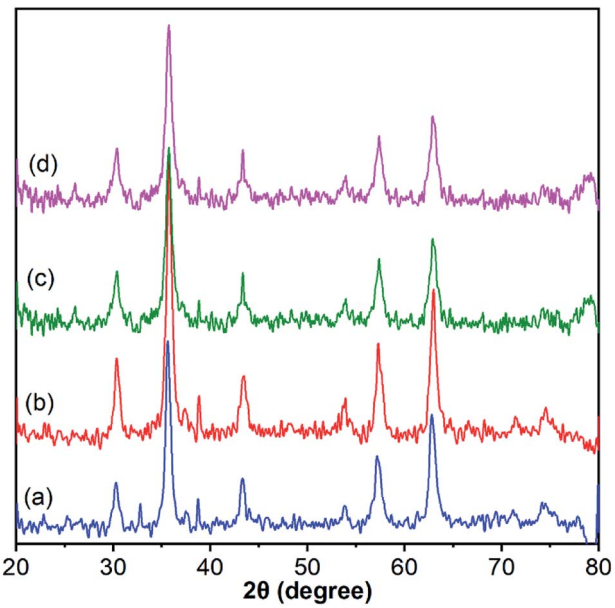

Fig. 5 X-Ray powder diffraction patterns for (a) Fe_3O_4, (b) Fe_3O_4@SiO_2, (c) Fe_3O_4@SiO_2@PTA(+) and (d) Fe_3O_4@SiO_2@PTA(−). The expanded spectra and related details have been shown in Fig. S6–S9.†

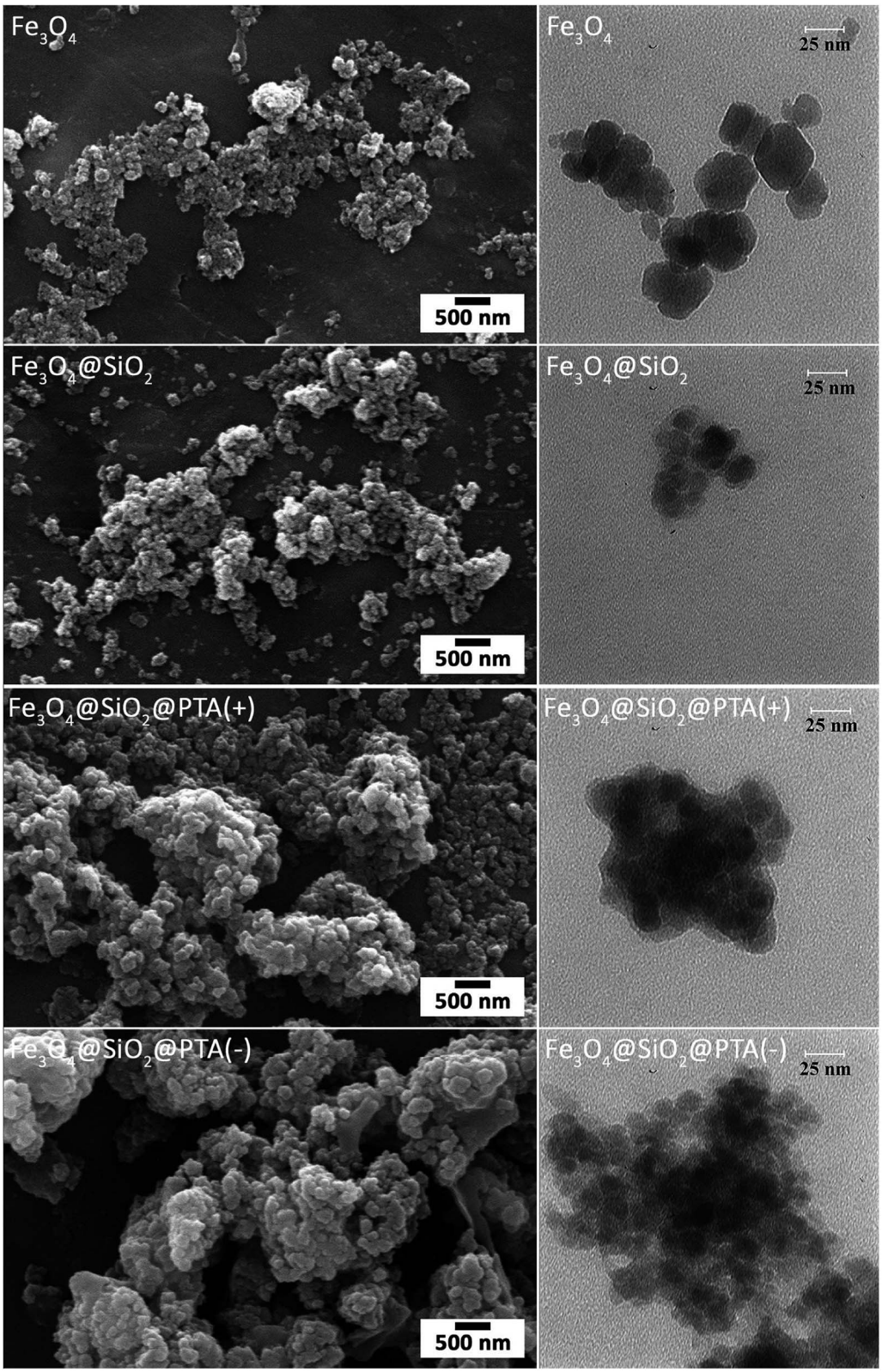

Fig. 6 SEM and TEM images of Fe_3O_4, Fe_3O_4@SiO_2, Fe_3O_4@SiO_2@PTA(+) and Fe_3O_4@SiO_2@PTA(−).

Direct separation of racemic compounds

Enantioseparation was carried out according to details specified in the experimental section for five racemic compounds (±)-α-methylbenzylamine, DL-tartaric acid, DL-alanine, DL-phenylalanine, and DL-valine. Before treatment with adsorbent, all five racemic compounds showed no optical activity because of the equal amounts of optical (+)

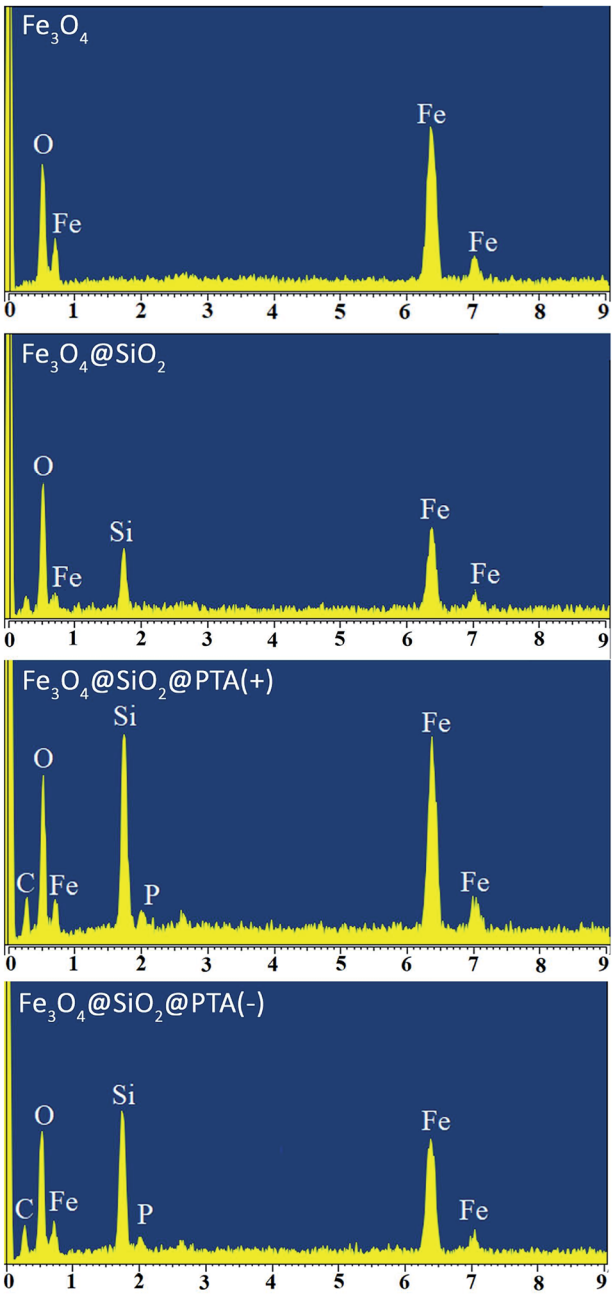

Fig. 7 EDX images of Fe_3O_4, Fe_3O_4@SiO_2, Fe_3O_4@SiO_2@PTA(+) and Fe_3O_4@SiO_2@PTA(−).

and (−) enantiomers in the solutions. The results of enantioseparation processes are given in Table 1 and the chemical structures of racemic compounds are shown in Scheme 2. The optical rotations for supernatants showed that Fe_3O_4@SiO_2@PTA(+) adsorbed (−) enantiomers of valine, alanine, tartaric acid and phenylalanine, and (+) enantiomer of α-methylbenzylamine, while Fe_3O_4@SiO_2@PTA(−) separated the other enantiomers (optical purities 18–82%). To study the possibility of cleavage of chiral selector in the presence of racemic mixture, NMR spectroscopy was typically done for the supernatant of the enantioseparation experiment including Fe_3O_4@SiO_2@PTA(+) in the presence of (±)-MBA

Table 1 Chiral separation of five racemic compounds with Fe_3O_4@SiO_2@PTA(+) and Fe_3O_4@SiO_2@PTA(−) adsorbents

	$[\alpha]_\lambda^{RT}$ (°)/O.P. (%)	
Samples	Fe_3O_4@SiO_2@PTA(+)	Fe_3O_4@SiO_2@PTA(−)
(±)-MBA	−16.8/82	+14.7/72
DL-Alanine	+8.9/79	−8.0/71
DL-Valine	+16.4/72	−14.1/62
DL-Tartaric acid	+2.4/19	−2.3/18
DL-Phenylalanine	+18.4/58	−20.1/63

solution. The ^{1}H-NMR and ^{13}C-NMR spectra merely showed the signals of α-methylbenzyl amine and the ^{31}P-NMR spectrum did not show any signal, which confirmed the stability of adsorbent in the racemic mixture. The ^{1}H-NMR spectrum is shown in Fig. S10.† The recycling of nano-composite adsorbents was also checked after ending the separation process. So, adsorbents were gathered by an external magnet, washed in a mixture of H_2O/CH_3OH under ultrasonic radiation for 10 min and dried in a vacuum oven for 12 h in 25 °C. Due to the release of the adsorbed enantiomer, the washing solution showed the optical rotatory.

Typically, the dried (+)-adsorbent was added to 25 mL of (±)-MBA solution (5 g L^{-1}, water/methanol 80/20, v/v) and continuously stirred for 1 h. After that, the specific rotation of solution changed to −10.1° showing that the chiral adsorbent can be recycled with little loss of activity. This slight loss of activity may be due to a few changes in the morphology of nanoparticles in the presence of H_2O/CH_3OH/(±)-MBA, which is usual for nano-compounds in the presence of chemicals, however, it was not further investigated.[53,80]

A comparison of chiral adsorbents presented here with other chiral Fe_3O_4@SiO_2-based adsorbents is given in Table 2. The Fe_3O_4@SiO_2@PTA(+) and Fe_3O_4@SiO_2@PTA(−) possess competitive advantages, such as high selectivity and recycling in the direct enantioseparation. Furthermore, we examined the racemic samples belonging to both acid and base families, which were successfully separated by these adsorbents. Preparation of both chiral (+) and (−) adsorbents is another advantage of this work, which helps to facilitate the separation process.

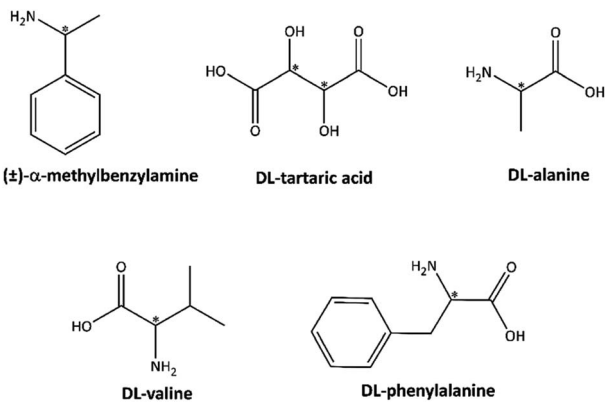

Scheme 2 Chemical structures of racemic mixtures.

Table 2 Comparison of chiral Fe_3O_4@SiO_2-based nano-adsorbents

Chiral adsorbents	Examined racemates	Optical purity (%)	Reference
Cellulose derivative-modified magnetic silica	(±)-2-Phenoxypropionic acid, benzoin methyl ether, promethazine hydrochloride	Above 80	57
Teicoplanin-modified magnetic silica microspheres	DL-Tryptophan, DL-phenylalanine, DL-mandelic acid, *N*-benzoyl-DL-alanine	8–35	53
β-CD modified magnetic silica microspheres	Dansyl DL-valine, dansyl DL-phenylalanine, dansyl DL-leucine	10–12	81
HSA modified magnetic silica microspheres	DL-Tryptophan	10–38	82 and 83
Fe_3O_4@SiO_2@PNCD	DL-Tryptophan	80	28
Fe_3O_4@SiO_2@PTA(+)	(±)-MBA, DL-alanine, DL-valine, DL-tartaric acid, DL-phenylalanine	18–82	This work
Fe_3O_4@SiO_2@PTA(−)			

Conclusion

Two single enantiomer nano-composites Fe_3O_4@SiO_2@PTA(+) and Fe_3O_4@SiO_2@PTA(−) were prepared and used for direct enantioseparation of some racemic mixtures. The racemates examined belong to both acid and base families. Excellent separation was achieved for examined basic racemic mixtures and comparative results were obtained for acidic ones with regard to previously reported Fe_3O_4@SiO_2-based adsorbents. The nanocomposites were characterized by FTIR, TEM, SEM, EDX, XRD, and VSM. The nanoparticles have a uniform shape with an average diameter of around 40–50 nm. The super-paramagnetic property is observed in nano-composites and is also stable after enantioseparation.

Conflicts of interest

The authors have no conflicts of interest regarding this work.

Acknowledgements

Authors gratefully acknowledge the financial support for this study by Ferdowsi University of Mashhad (Project No. 41927/3).

References

1 G. N. Sas, *9.17 Industrial Applications of Chiral Chromatography*, 2012, vol. 9.
2 G.-Q. Lin, Q.-D. You and J.-F. Cheng, *Chiral drugs: chemistry and biological action*, John Wiley & Sons, 2011.
3 N. C. P. de Albuquerque, D. B. Carrão, M. D. Habenschus and A. R. M. de Oliveira, *J. Pharm. Biomed. Anal.*, 2018, **147**, 89–109.
4 F. He, Y. L. Qian and M. C. Qian, *Food Chem.*, 2018, **239**, 622–630.
5 K. W. Smith, S. Link and W.-S. Chang, *J. Photochem. Photobiol., C*, 2017, **32**, 40–57.
6 D. S. Bradshaw, J. M. Leeder, M. M. Coles and D. L. Andrews, *Chem. Phys. Lett.*, 2015, **626**, 106–110.
7 K. Itoh, F. Odate, T. Karikomi, K. Obe, T. Miyamori, H. Kamiya, K. Yoza, K. Nagai, H. Fujii and H. Suga, *RSC Adv.*, 2019, **9**, 12365–12369.
8 Y. Miyagi, T. Sotani, T. Yajima, N. Sano and F. Sanda, *Polym. Chem.*, 2018, **9**, 1772–1779.
9 Q. Zhang and L. Zhao, *Tetrahedron Lett.*, 2018, **59**, 310–316.
10 N. Yoshinari and T. Konno, *Bull. Chem. Soc. Jpn.*, 2018, **91**, 790–812.
11 G. D'Orazio, C. Fanali, M. Asensio-Ramos and S. Fanali, *TrAC, Trends Anal. Chem.*, 2017, **96**, 151–171.
12 Z. Shedania, R. Kakava, A. Volonterio, T. Farkas and B. Chankvetadze, *J. Chromatogr. A*, 2018, **1557**, 62–74.
13 R. S. Hegade, M. De Beer and F. Lynen, *J. Chromatogr. A*, 2017, **1515**, 109–117.
14 J. Martens and R. Bhushan, *J. Pharm. Biomed. Anal.*, 1990, **8**, 259–269.
15 O. Jurček, M. Wimmerová and Z. Wimmer, *Coord. Chem. Rev.*, 2008, **252**, 767–781.
16 J. J. Keating, S. Bhattacharya and G. Belfort, *J. Membr. Sci.*, 2018, **555**, 30–37.
17 C. Meng, Y. Sheng, Q. Chen, H. Tan and H. Liu, *J. Membr. Sci.*, 2017, **526**, 25–31.
18 T. Gumí, C. Minguillón and C. Palet, *Polymer*, 2005, **46**, 12306–12312.
19 S. Marchesan, C. D. Easton, K. E. Styan, L. J. Waddington, F. Kushkaki, L. Goodall, K. M. McLean, J. S. Forsythe and P. G. Hartley, *Nanoscale*, 2014, **6**, 5172–5180.
20 L. Wang, K. Yu, B.-B. Zhou, Z.-H. Su, S. Gao, L.-L. Chu and J.-R. Liu, *Dalton Trans.*, 2014, **43**, 6070–6078.
21 Y. Dai, S. Wang, J. Zhou, Y. Liu, D. Sun, J. Tang and W. Tang, *J. Chromatogr. A*, 2012, **1246**, 98–102.
22 Z. Shedania, R. Kakava, A. Volonterio, T. Farkas and B. Chankvetadze, *J. Chromatogr. A*, 2018, **1557**, 62–74.
23 R. Gutierrez-Climente, A. Gomez-Caballero, A. Guerreiro, D. Garcia-Mutio, N. Unceta, M. A. Goicolea and R. J. Barrio, *J. Chromatogr. A*, 2017, **1508**, 53–64.
24 G.-H. Zhang, S. Liang, S. Tang, W. Chen and Z.-W. Bai, *Anal. Methods*, 2019, **11**, 1604–1612.
25 R. Wang, Y. Zheng, X. Li, J. Chen, J. Cui, J. Zhang and X. Wan, *Polym. Chem.*, 2016, **7**, 3134–3144.
26 B. Kafková, Z. Bosáková, E. Tesařová and P. Coufal, *J. Chromatogr. A*, 2005, **1088**, 82–93.
27 Y. Li, X. Chen and N. Gu, *J. Phys. Chem. B*, 2008, **112**, 16647–16653.
28 Y. K. Ye and R. W. Stringham, *Chirality*, 2006, **18**, 519–530.

29 L. Guo, Y. Song, H. Yu, L. Pan and C. Cheng, *Appl. Surf. Sci.*, 2017, **407**, 82–92.
30 J. S. Beck, J. C. Vartuli, W. J. Roth, M. E. Leonowicz, C. T. Kresge, K. D. Schmitt, C. T. W. Chu, D. H. Olson, E. W. Sheppard and S. B. McCullen, *J. Am. Chem. Soc.*, 1992, **114**, 10834–10843.
31 Y. Yu, L. Yu, K. Shih and J. P. Chen, *J. Colloid Interface Sci.*, 2018, **521**, 252–260.
32 W. Cai, M. Guo, X. Weng, W. Zhang and Z. Chen, *Mater. Sci. Eng., C*, 2019, **98**, 65–73.
33 M. Shao, F. Ning, J. Zhao, M. Wei, D. G. Evans and X. Duan, *J. Am. Chem. Soc.*, 2012, **134**, 1071–1077.
34 T. Zhao, X. Zhu, C.-T. Hung, P. Wang, A. Elzatahry, A. A. Al-Khalaf, W. N. Hozzein, F. Zhang, X. Li and D. Zhao, *J. Am. Chem. Soc.*, 2018, **140**, 10009–10015.
35 Y. Li, J. J.-Y. Suen, E. Prince, E. M. Larin, A. Klinkova, H. Thérien-Aubin, S. Zhu, B. Yang, A. S. Helmy and O. D. Lavrentovich, *Nat. Commun.*, 2016, **7**, 12520.
36 Z. Asgharpour, F. Farzaneh and A. Abbasi, *RSC Adv.*, 2016, **6**, 95729–95739.
37 C. Maccato, G. Carraro, D. Peddis, G. Varvaro and D. Barreca, *Appl. Surf. Sci.*, 2018, **427**, 890–896.
38 N. Liang, X. Hou, P. Huang, C. Jiang, L. Chen and L. Zhao, *Sci. Rep.*, 2017, **7**, 13844.
39 Q. Gao, W. Xie, Y. Wang, D. Wang, Z. Guo, F. Gao, L. Zhao and Q. Cai, *RSC Adv.*, 2018, **8**, 4321–4328.
40 H. Bagheri, N. Pajooheshpour, A. Afkhami and H. Khoshsafar, *RSC Adv.*, 2016, **6**, 51135–51145.
41 S. Tural, B. Tural, M. Ş. Ece, E. Yetkin and N. Özkan, *J. Sep. Sci.*, 2014, **37**, 3370–3376.
42 Q. Wei, P. Song, Z. Yang and Q. Wang, *Phys. E*, 2018, **103**, 156–163.
43 S. R. Firoozabadi, M. Bonyadi and A. Lashanizadegan, *J. Nat. Gas Sci. Eng.*, 2018, **59**, 374–386.
44 Q. Zheng, Z. R. Zhang, J. Du, L. L. Lin, W. X. Xia, J. Zhang, B. R. Bian and J. P. Liu, *J. Mater. Sci. Nanotechnol.*, 2019, **35**, 560–567.
45 M. Gadhvi, *Mater. Sci. Eng., B*, 2010, **168**, 106–110.
46 X. Deng, W. Li, G. Ding, T. Xue and X. Chen, *Sep. Purif. Rev.*, 2019, **48**, 14–29.
47 W. Wang, B. Tang, B. Ju, Z. Gao, J. Xiu and S. Zhang, *J. Mater. Chem. A*, 2017, **5**, 958–968.
48 X. Liu, Z. Ma, J. Xing and H. Liu, *J. Magn. Magn. Mater.*, 2004, **270**, 1–6.
49 B. Tural, E. Ertaş and S. Tural, *Desalin. Water Treat.*, 2016, **57**, 26153–26164.
50 B. Tural, E. Ertaş, B. Enez, S. A. Fincan and S. Tural, *J. Environ. Chem. Eng.*, 2017, **5**, 4795–4802.
51 S. Tural, M. Ş. Ece and B. Tural, *Ecotoxicol. Environ. Saf.*, 2018, **162**, 245–252.
52 Y. Wei, A. Tian, Y. Li, X. Wang and B. Cao, *J. Mater. Chem.*, 2012, **22**, 8499–8504.
53 J. Wu, P. Su, J. Huang, S. Wang and Y. Yang, *J. Colloid Interface Sci.*, 2013, **399**, 107–114.
54 H. J. Choi and M. H. Hyun, *Chem. Commun.*, 2009, 6454–6456.
55 K. Li, Z. Zeng, J. Xiong, L. Yan, H. Guo, S. Liu, Y. Dai and T. Chen, *Colloids Surf., A*, 2015, **465**, 113–123.
56 L.-Y. Guo, S.-Y. Zeng, Z. Jagličić, Q.-D. Hu, S.-X. Wang, Z. Wang and D. Sun, *Inorg. Chem.*, 2016, **55**, 9006–9011.
57 J. M. Chem, Y. Wei, A. Tian, Y. Li, X. Wang and B. Cao, *J. Mater. Chem.*, 2012, **22**, 8499–8504.
58 T. Tarhan, B. Tural, S. Tural and G. Topal, *Chirality*, 2015, **27**, 835–842.
59 E. Torabi Farkhani, M. Pourayoubi, M. Izadyar, P. V. Andreev and E. S. Shchegravina, *Acta Crystallogr., Sect. C: Struct. Chem.*, 2018, **74**, 847–855.
60 B. Vahdani Alviri, M. Pourayoubi, A. Farhadipour, M. Nečas and V. Bertolasi, *Acta Crystallogr., Sect. C: Struct. Chem.*, 2018, **74**, 1610–1621.
61 F. Sabbaghi, M. Pourayoubi, M. Nečas and K. Damodaran, *Acta Crystallogr., Sect. C: Struct. Chem.*, 2019, **75**, 77–84.
62 S. Akbari, R. S. Khoshnood, F. Karimi Ahmadabad, M. Pourayoubi, M. Dušek and E. S. Shchegravina, *RSC Adv.*, 2019, **9**, 9153–9159.
63 F. Karimi Ahmadabad, M. Pourayoubi and H. Bakhshi, *J. Appl. Polym. Sci.*, 2019, **136**, 48034.
64 B. Vahdani Alviri, M. Pourayoubi, A. Saneei, M. Keikha, A. Van Der Lee, A. Crochet, A. A. Ajees, M. Nečas, K. M. Fromm, K. Damodaran and T. A. Jenny, *Tetrahedron*, 2018, **74**, 28–41.
65 F. H. Allen, *Acta Crystallogr., Sect. B: Struct. Sci.*, 2002, **58**, 380–388.
66 C. R. Groom, I. J. Bruno, M. P. Lightfoot and S. C. Ward, *Acta Crystallogr., Sect. B: Struct. Sci., Cryst. Eng. Mater.*, 2016, **72**, 171–179.
67 F. Sabbaghi, M. Dušek, S. Bayat and M. Nečas, *Struct. Chem.*, 2016, **27**, 1831–1844.
68 M. Pourayoubi, F. Karimi Ahmadabad, H. Eshtiagh-Hosseini, M. Kučeráková, V. Eigner and M. Dušek, *Acta Crystallogr., Sect. C: Cryst. Struct. Commun.*, 2013, **69**, 1181–1185.
69 M. Toghraee, M. Pourayoubi and V. Divjakovic, *Polyhedron*, 2011, **30**, 1680–1690.
70 A. Tarahhomi, M. Pourayoubi, J. A. Golen, P. Zargaran, B. Elahi, A. L. Rheingold, M. A. Leyva Ramírez and T. Mancilla Percino, *Acta Crystallogr., Sect. B: Struct. Sci., Cryst. Eng. Mater.*, 2013, **69**, 260–270.
71 U. Holzwarth and N. Gibson, *Nat. Nanotechnol.*, 2011, **6**, 534.
72 X. Liu, Z. Ma, J. Xing and H. Liu, *J. Magn. Magn. Mater.*, 2004, **270**, 1–6.
73 M. Keikha, M. Pourayoubi, A. Tarahhomi and A. van der Lee, *Acta Crystallogr., Sect. C: Struct. Chem.*, 2016, **72**, 251–259.
74 M. Eghbali Toularoud, M. Pourayoubi, M. Dušek, V. Eigner and K. Damodaran, *Acta Crystallogr., Sect. C: Struct. Chem.*, 2018, **74**, 608–617.
75 S. Radi, S. Tighadouini, M. Bacquet, S. Degoutin, F. Cazier, M. Zaghrioui and Y. N. Mabkhot, *Molecules*, 2013, **19**, 247–262.
76 H. Naeimi, Z. S. Nazifi and Z. Sadat, *J. Nanopart. Res.*, 2013, **15**, 2026.
77 L.-D. Guo, Y.-Y. Song, H.-R. Yu, L.-T. Pan and C.-J. Cheng, *Appl. Surf. Sci.*, 2017, **407**, 82–92.

78 T. Kieu, H. Ta, M. Trinh, N. V. Long, T. Thanh, M. Nguyen, T. Lien, T. Nguyen, T. L. Thuoc, B. T. Phan, D. Mott, S. Maenosono, H. Tran-van and V. H. Le, *Colloids Surf., A*, 2016, **504**, 376–383.

79 T. Yang, C. Shen, Z. Li, H. Zhang, C. Xiao, S. Chen, Z. Xu, D. Shi, J. Li and H. Gao, *J. Phys. Chem. B*, 2005, **109**, 23233–23236.

80 F. Karimi Ahmadabad, M. Pourayoubi and H. Bakhshi, *Mater. Chem. Phys.*, 2017, **199**, 79–87.

81 J. Wu, P. Su, D. Guo, J. Huang and Y. Yang, *New J. Chem.*, 2014, **38**, 3630–3636.

82 F. Edwie, Y. Li and T.-S. Chung, *J. Membr. Sci.*, 2010, **362**, 501–508.

83 J. Wu, P. Su, Y. Yang, J. Huang, Y. Wang and Y. Yang, *J. Mater. Chem. B*, 2014, **2**, 775–782.